Monitoring damage evolution of ceramic matrix composites during tensile tests using electrical resistivity: Crack density-based electromechanical model

J.P. Goulmy, G. Camus, F. Rebillat

Laboratoire des Composites Thermostructuraux,

Université de Bordeaux et CNRS/SAFRAN/CEA

3 allée de la Boétie, 33600 Pessac, France

Corresponding author :

goulmy@lcts.u-bordeaux.fr (J.P. Goulmy)

(+33) 4 42 93 82 23

Abstract

In order to further develop and understand the data provided by electrical resistance measurements, three ceramic matrix composites (CMCs) were characterized in tension. The observed changes of the electrical resistance were compared to the acoustic emission spectra, another commonly used damage monitoring method, as well as the classical interposed unloading/reloading cycles. A model was then proposed in order to predict the evolution of the resistance as a function of the damage state of the three composites. The proposed model provides accurate results for the three materials which, although they all belong to the CMC family, display different mechanical and physical behaviors.

Keywords

Ceramic Matrix Composites (CMCs); electrical resistivity; acoustic emission spectra; tensile tests; damage monitoring

1. Introduction

The excellent thermo-mechanical properties of ceramic matrix composites have led to many developments regarding their use inside aeronautical jet engines [1–3]. The non-brittle mechanical behavior of these composites made of brittle constituents is brought by various energy dissipating mechanisms collectively termed as damage, such as matrix micro-cracking and concomitant debonding and sliding. These mechanisms are enhanced and controlled by coating the fibers with a so called interphase (a compliant material being mostly carbon and boron nitride (BN)).

It is therefore essential to develop non-destructive techniques able to follow the onset and propagation of damage, which can be applied to structural components displaying complex geometries. A wide range of non-destructive techniques has been evaluated for being used with CMCs [4]. Techniques using either ultrasonic or X-ray signals as well as pulsed thermography, however, usually require the component to be taken out of service for quite long durations. The recording of acoustic emission signals has proved to be efficient for quantifying matrix cracking in CMCs but is less sensitive to debonding and sliding related crack opening [5].

After having been widely used with metallic alloys and with carbon fiber-reinforced polymer composites (CFRP) [6,7], electrical resistance monitoring (ER) has been recently adapted and applied to CMCs [8–17]. The ER technique allows to follow the onset and propagation of damage in the material, most particularly the one associated to the most conductive phase when it is subjected to crack opening (which tends to interrupt the current flow and thus to increase the electrical resistance). For example, regarding melt-infiltrated (MI) SiC/SiC materials with a BN interphase, it has been found that the highly conductive free silicon phase present in the matrix mainly drives the resistivity of the composites [10,15]. Conversely, for any C/SiC composite possessing a pyrocarbon interphase (i.e. C/C/SiC composite), both the fibers and the interphase are the most conductive phases (as it is highlighted in the next section).

In order to be able to link the damage related nonlinear mechanical behavior of these CMCs to the evolution of their electrical resistance, different models have been proposed in

2

the literature [10,12,18,19]. These models, all inspired by those first set up with CFRP composite, were based on the coupling between electrical resistance networks and mechanical shear-lag models, introducing an "electrically inefficient length". An analytical model, firstly proposed by Sujidkul et al. [19] and modified by Morscher et al. [10] in order to take into account transverse matrix cracking instead of fiber failure, was applied to MI composites with a BN interphase. This model allowed to obtain excellent results up to matrix cracks saturation. More recently, work has been carried out on a SiC/C/SiBC composite [12], using a model based on a similar electrical network but mainly distinguished by the use of Hutchinson equations to link mechanical and electrical properties. Finally, one should also mention the recent development of a numerical model, aimed at applying the finite element method to quantify the effect of specific damage states on the ER response of a melt infiltrated SiC/SiC composite [20].

The objectives of this study are (i) to investigate the influence of the nature of the CMC on the changes observed in the electrical resistivity measurements performed during a tensile test and (ii) to propose a general model for CMCs relating their mechanical behavior to their electrical resistance. For this purpose, three CMCs of several natures, namely a C/C/SiC, a SiC/C/SiBC and a SiC/BN/SiC (further referred to as SiC/BN/SiC-Si to highlight the importance of residual Si), have been used. The main interest with the use of these composites is that their most conducting constituent is always different.

2. Materials and methods

Three different continuous fiber reinforced ceramic matrix composites, all manufactured by SAFRAN Ceramics using woven interlock fibrous preforms have been tested in tension at room temperature. The material denominated SiC/C/SiBC is based on a SiC Nicalon NL207 fiber coated with a pyrocarbon interphase, the matrix being composed of ex-polymer SiC and CVI processed [SI-B-C] layers (with self-healing capacities). A second composite, denominated SiC/BN/SiC-Si, uses Hi-Nicalon S fibers coated with a BN interphase. The matrix has been processed with the melt-infiltration technique, and is therefore composed of a SiC phase and a portion of free Si. The last composite, mentioned as C/C/SiC all along the text,

uses PANEX carbon fibers, coated with a pyrocarbon interphase, the SiC matrix being fully processed by CVI.

Micrographs of the as-received composites, obtained through optical microscopy observations performed on polished samples, are displayed in Figure 1. The two materials mainly processed by CVI exhibit macropores with sharp singularities in the interbundle matrix-rich region. Conversely, the MI composite does not display such macroporosity which has been almost fully filled up by the dual SiC-Si matrix.
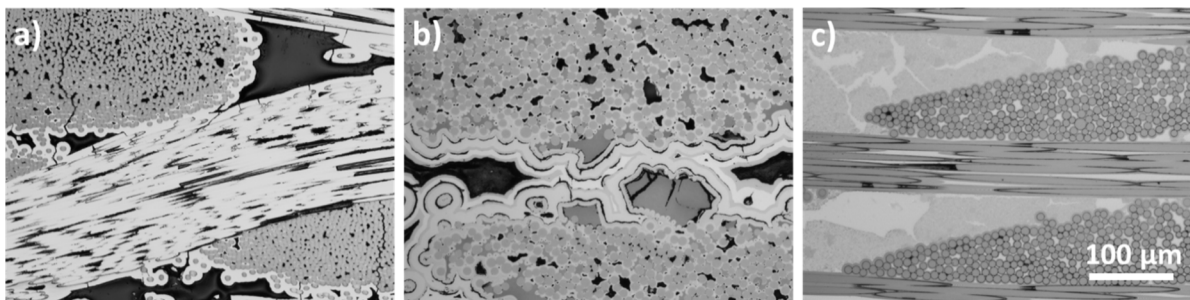

Figure 1. Microstructural characterizations of the as-received composites, a) C/C/SiC composite, b) SiC/C/SiBC composite, and c) SiC/BN/SiC-Si composite.

All the specimens machined from composite plates were tested in tension on an Instron 4505 machine at a constant displacement rate of 0.3mm/min with interposed unloading/reloading cycles, using hydraulic grips. Prior to testing, samples were equipped with glass fiber-reinforced epoxy tabs, in order (i) to avoid an extra damage linked to the clamping pressure and (ii) to provide an electrical insulation from the testing system. Two extensometers (25mm) were placed on the opposite edges in order to check for possible bending/torsion components intervening during the test.

It is worthy of note that, although test samples had somewhat various shapes and sizes since they were supplied at different times for different purposes, the similar slow displacement rate used experimentally always ensured quasi-static loading conditions. This point, added to the fact that both the gage length of the extensometers and the cross-section of the samples were largely coherent with the elementary representative volume (ERV) of the composites, has allowed to directly compare the stress-strain behaviors.

It should also be mentioned that, because of their limited availability, only two samples of each composite material were tested. Since results of the tests, displayed and discussed in

the next paragraph, have shown no significant scattering (see figure 2), the behavior of only one of these two samples is systematically reported.

Electrical resistance (ER) was measured using a four-point probe method in order to minimize contact resistance. Two rings were first pasted around the specimen with CW2400 conductive epoxy, in order to collect the surface current on the whole perimeter of the samples. Shallow grooves were machined in the edges at the extremities of the samples so that the outer wires could be set in the right place, and then fixed using CW2400 conductive epoxy. A constant direct current was applied through the outer wires whereas the associated voltage was measured between the inner wires [12].

Typical resistivity values of the material constituents are reported in table 1. The resistivity ρ is deduced from the gage resistance R according to the formula $\rho = RS/L_g$ (where S is the average cross-section between the gage leads and L_g is the length between the two contacts). This formula reveals a fair way of compiling normalized values, which may thus be directly compared. It appears that the pyrocarbon interphase is the most conductive constituent in the case of SiC/C/SiBC composite whereas, conversely, the matrix is the most conductive constituent in the case of the SiC/BN/SiC-Si material. On the other hand, carbon fibers and pyrocarbon interphase are the most conductive constituents in the case of the C/C/SiC composite. Since these constituents account for more than 50% of the composite volume fraction, a low electric resistance increase was expected, which justifies that a different measurement method was developed for this material.

Recording of resistance was performed with an Agilent 3644A provided a current of 500 mA for the C/C/SiC composite and a current of 100 mA for both SiC/C/SiBC and SiC/BN/SiC-Si composites, and a voltmeter (HP 3852) measured the induced voltage. The stability of the measurements was checked during 24 hours once the samples were fixed in the hydraulic jaws and left at room temperature without any loading being applied. With this system, the electrical resistance was measured with an accuracy of 5 10^{-3} mΩ.

It is finally worth mentioning that electric resistance variations are always reported in a relative manner all along the text (i.e. $\Delta R/R_0$ as a function of strain), which allows to get rid of possible problems when comparing values obtained from samples of different shapes and sizes.

Acoustic emission signals were additionally recorded, using a MISTRAS Group SA system, equipped with a PICO sensors pasted on the specimens. Data were recorded at a rate of 2 MHz, and the detection threshold was fixed to 45 dB.

C/C/SiC			
Constituents	C fiber	SiC matrix	PyC
Resistivity (Ω.m)	$1.7\ 10^{-5}$	$10^3 - 10^5$	$1.5\ 10^{-5} - 4.5\ 10^{-5}$
Typical surface in the composite relative to PyC surface (order of magnitude)	10	20	1
ρ/ρ(PyC) (order of magnitude)	0.5	10^3	1
SiC/C/SiBC			
Constituents	NL207 fiber	SiC matrix	PyC
Resistivity (Ω.m)	9 - 10	$10^3 - 10^5$	$1.5\ 10^{-5} - 4.5\ 10^{-5}$
Typical surface in the composite relative to PyC surface (order of magnitude)	20	20	1
ρ/ρ(PyC) (order of magnitude)	10^4	10^3	1
SiC/BN/SiC-Si			
Constituents	NL207 fiber	SiC-Si SiC matrix	BN
Resistivity (Ω.m)	9 - 10	$7.45\ 10^{-5}$ [20]	$0.6\ 10^{-3} - 3$
Typical surface in the composite relative to MI SiC/Si surface (order of magnitude)	1.15	1	0.2
ρ/ρ(MI SiC/Si) (order of magnitude)	10	1	10^3

Table 1. Typical resistivity values of the materials constituents as found in the literature [21,22,10,20,12].

3. Results and discussion

The initial resistance values of the three materials, R_0, are given in Table 2, along with their initial resistivity ρ_0. It may be seen that the SiC/BN/SiC-Si composite presents an initial resistivity ten times lower than that of the SiC/C/SiBC composite, most certainly because the conductive silicon is present in a significant proportion in the matrix, in contrast with the proportion of C in the case of the SiC/C/SiC composite. It may also be seen that the C/C/SiC composite has a much lower resistivity than the other two materials (of in the order of 10^{-5} Ω.m), in accordance with what was expected from the values of its constituents.

Table 2 also displays an average measure of the resistance values reached by the three specimens slightly before failure. It clearly appears that the variations in resistance observed during the tests are dependent on the type of composite, the greatest variation being obtained with the SiC/BN/SiC-Si material (about 250%) while the SiC/C/SiBC composite has a 60% increase in resistance and the C/C/SiC displays only 4% of increase.

Composite material	C/C/SiC	SiC/C/SiBC	SiC/BN/SiC-Si
Length between contacts / cross-section (mm^{-1})	5	4	2.5
Initial resistance R_0 (Ω)	0.0507	1.07	0.08
Initial resistivity ρ_0 (Ω.m)	$3\ 10^{-5} \pm 5\ 10^{-6}$	$1.08\ 10^{-3} \pm 2\ 10^{-4}$	$1.02\ 10^{-4} \pm 1\ 10^{-5}$
R at failure (Ω)	0.0528	1.72	0.30
R-R0 at failure (Ω)	0.00210	0.65	0.21246

Table 2. Electrical values (resistance and resistivity) before and after testing the three composites.

Figure 2 shows the stress/strain curves along with the evolution of the acoustic emission signal for the three materials (normalized by the maximum value reached during the test). All these curves display a more or less extended linear domain followed by a non-linear behavior up to rupture. Permanent strains are observed upon complete unloading for the SiC/C/SiBC and the C/C/SiC composites whereas, in the case of the SiC/BN/SiC-Si composite, they are almost non-existent. These curves highlight two other important facts observed for the three materials: (i) a gradual decrease of the average modulus provided by the unloading/reloading cycles interposed in the nonlinear domains and (ii) a hysteretic behavior of these cycles, in relation with the various frictional phenomena accompanying matrix micro-cracking. The permanent strains observed for the C/C/SiC and SiC/C/SiBC composites result from transverse micro-cracks (i.e. perpendicular to the loading direction) which are incompletely closed, because of the unrecoverable energy, *i.e.* the one dissipated by the damage processes and because of the release of the residual stresses introduced by the various processing steps. In the case of the C/C/SiC composite, the difference in thermal expansion coefficients between the carbon fibers and the matrix is sufficiently elevated to generate significant tensile residual stresses during cooling from the high temperature manufacturing process. The partial release of these residual stresses resulted in (i) the presence of cracks inside the matrix (see Figure 1) and (ii) a concurrent point of the slopes of the equivalent modulus (derived from the unloading/reloading cycles) situated in the compression domain [23]. On the other hand, nearly no permanents strains are observed in the case of the SiC/BN/SiC-Si composite whereas the slopes of the equivalent modulus provided by the unloading/reloading cycles happen to be concurrent at a single point situated in the tensile domain. This information indicates that residual compression strains are likely to be present within the matrix. All these observations are also in good agreement with the low yield stress of 25 MPa observed for the C/C/SiC composite as compared to the value of 275 MPA observed for the SiC/BN/SiC-Si composite.

The acoustic emission curves of the C/C/SiC and SiC/BN/SiC-Si composites present the classical sigmoidal evolution frequently observed, ending with a more or less asymptotic

behavior representative of the saturation of matrix cracking. For the SiC/C/SiBC material, an increase in the acoustic emission rate is observed at the end of the test, which may be attributed to progressive fiber breakage. It is also important of note that no activity is present during the unloading/reloading cycles, which indicates that no damage takes place upon cycling.

For the three materials, the monotonic relative evolutions of the electrical resistance during the tests, displayed in Figure 3, are comparable. After a small increase mainly related to the variation in strain and therefore to the piezoelectric character of the material, a strong increase up to rupture is always observed. This increase is undoubtedly linked to the multiplication and above all to the opening of the matrix micro-cracks.

Permanent electric resistances are observed upon complete unloading for the three materials, thus indicating that there are micro-cracks which are incompletely closed. The remarkable fact is that, while this is coherent with the permanent strains exhibited by the C/C/SiC and SiC/C/SiBC composites, this is apparently no longer the case with the SiC/BN/SiC-Si composite for which these permanent strains are negligible. There is therefore a damage entity which remains active from an electrical point of view but which has no influence on the longitudinal strains. In the case of these two composites, all the studies previously performed have shown that most of the micro-cracks are perpendicular to the loading direction so that their opening/closure may be followed by the longitudinal contact extensometers presently used. Conversely, it has been shown that micro-cracks longitudinal to the loading direction are largely present in the SiC/BN/SiC-Si composite [24].

Even if the opening of these micro-cracks cannot be evidenced by longitudinal extensometers, a discontinue interface is present when this crack is fully closed and may be responsible for the noticeable permanent electrical resistances of the SiC/BN/SiC-Si composites.
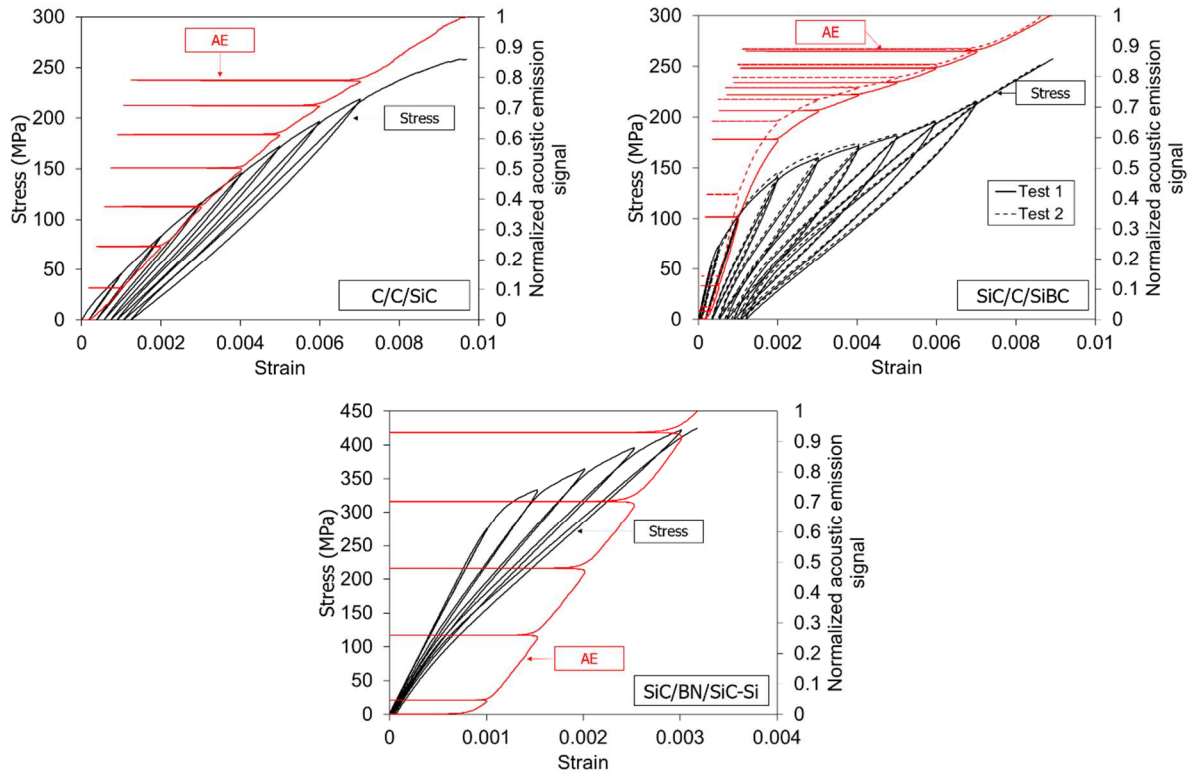
Figure 2. Tensile behavior of the three materials with interposed unloading/reloading cycles and the normalized acoustic emission signal. Comparison of the two tests performed for the composite SiC/C/SiBC.
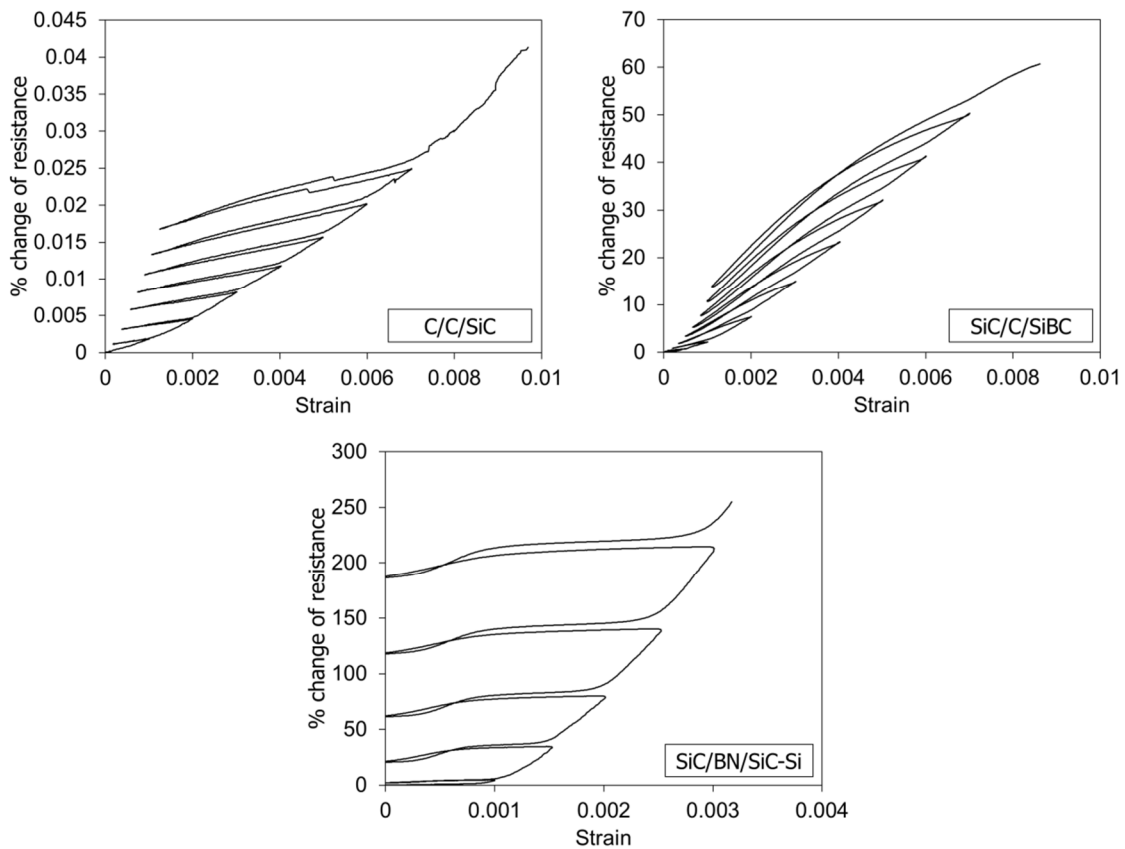

Figure 3. Evolution of the electrical resistance as a function of the strain level, for tension tests performed on the three composites with interposed unloading/reloading cycles.

4. Modeling of the electrical resistance changes

4.1.   *The electromechanical model*

Electromechanical models have been previously proposed in the literature, particularly for the SiC/C/SiBC material used in this work [12,20]. The model of the elementary cell and its application to a domain consisting of a finite number of these cells, see Figure 4, resulted in the following equation which expresses the relative resistance variation as a function of strain[12,19][12,19] :

$$\frac{\Delta R(\varepsilon)}{R_0} = (1 + \alpha_0.\varepsilon)\left[\frac{2l_d}{\delta}\left(\frac{\phi_d - \phi_s}{\phi_s}\right).\rho_c(\varepsilon) + 1\right] - 1 \qquad \textbf{Eq. 1}$$

With α_0 being the piezoresistance factor of the undamaged composite, l_d half the length of the debonded zone in the unit cell, δ the length of the unit cell, ϕ_s the resistivity of the undamaged unit cell, ϕ_d the resistivity of the fully damaged unit cell and ρ_c the matrix crack density (0< ρ_c <1).

Remark: it is worth mentioning that, when considering (i) the relationship between the resistance and the resistivity (i.e. $\rho = RS/L_g$) and (ii) the extremely small changes encountered by the transverse strains during the tensile tests (i.e. the cross-section S remains close to its initial value S_0), changes in the relative resistance and in the relative resistivity remain almost identical.

By considering the parameter L_d which represents the debonding density, proportional to l_d/δ, a constant term K was then introduced so that Eq. 1 could be rewritten as:

$$\frac{\Delta R(\varepsilon)}{R_0} = (1 + \alpha_0.\varepsilon)[K.L_d(\varepsilon).\rho_c(\varepsilon) + 1] - 1 \qquad \textbf{Eq. 2}$$
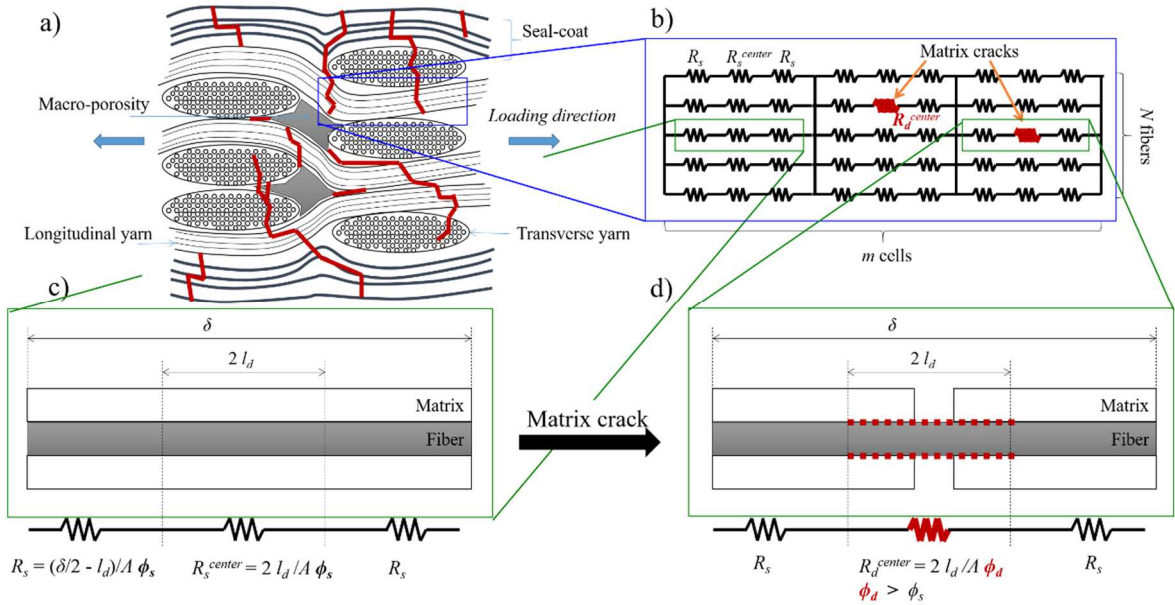
Figure 4. Schematic representation of (a) the damaged SiC/C/SiBC material loaded at a strain of around 0.5% with crack propagation in the seal-coat, in the inter-tow matrix, in the transverse tows and in the longitudinal tows, (b) an electrical network of multiple parallel cells in series representing the cracked composite, (c) the initial unit cell and (d) the same cell with a matrix crack and a debonded interfaces [12].

This is the hypothesis of a unique type of microcracking as usually encountered in 1D composites, which allowed to consider coefficients K and α_0 being constant (*i.e.* unaffected by damage). This last coefficient was estimated from the initial slope of the resistivity/strain curve. In order to identify K, by reversing Eq. 2 with the help of the experimental values found for the evolution of the electrical resistance, one had first to estimate $L_d(\varepsilon)$ and $\rho_c(\varepsilon)$.

This was done by using values extracted from the unloading/reloading cycles of the stress/strain curve and a micromechanical model derived from the work of Hutchinson el al. [12,25,26]. It has be noticed that these so-called Hutchinson's equations, only qualitatively suitable for being used with 1D composites (in fact microcomposites constituted by a single fiber coated with a matrix, since no mathematical homogenization was added). However, they provided good results with the 2D interlock SiC/C/SiBC composite used in the study of Simon et al. One should however consider that this is mainly because the electrical resistance of this composite is strongly governed by the pyrocarbon interphase of the longitudinal tows [12]. This fact is however unlikely to be true with any multi-directionally reinforced CMC when considering their general damaging process [27]. More particularly, for the C/C/SiC and the SiC/BN/SiC-Si of the present study, carbon fibers on one hand and

11

residual Si on the other hand are also present elsewhere than in longitudinal tows: the electrical resistance should therefore be also impacted by the damage phenomena taking place in the inter-tow matrix and in the transverse tows.

It is therefore proposed to setup a generalization of the electromechanical model, suitable to different CMCs (at least those used in the present study). The basic conjecture is that Eq. 2 remains valid if one uses non-constant terms K and α, *i.e.* being functions of the strain ε. This hypothesis is justified by the fact that the model of the elementary cell, illustrated by Figure 4, remains pertinent for any kind of damaging process (*i.e.* within the inter-tow matrix, within the transverse tows and within the longitudinal tows) but with different values for α_0 and for the term $\frac{2l_d}{\delta}\left(\frac{\phi_d-\phi_s}{\phi_s}\right)$.

The following equation has thus to be considered:

$$\frac{\Delta R(\varepsilon)}{R_0} = (1 + \alpha(\varepsilon).\varepsilon)[K(\varepsilon).L_d(\varepsilon).\rho_c(\varepsilon) + 1] - 1 \qquad \text{Eq. 3}$$

The electrical resistance variation, *ΔR(ε)*, being experimentally determined, one has then to identify the remaining functions.

In this respect, it has been assumed, as a second hypothesis, that the microcracks density ρ_c is proportional either to the evolution of the usual damage parameter d related to the elastic modulus (*i.e. d = 1 − E/E₀*), identified with the unloading/reloading cycles (at the beginning of unloading [28,29]) or from the acoustic emission signal S_{AE} (which may be recorded and used either in term of number of hits or of energy).

$$\rho_c(\varepsilon) = k\, d(\varepsilon) \qquad \text{Eq. 4}$$

$$\rho_c(\varepsilon) = q\, S_{AE}(\varepsilon)$$

Among these two possibilities, the second one appears to be more attractive for the acoustic signal is continuously recorded, as is the electrical resistance variation. However, if the parameter k is constant by definition (*i.e. d* is set up with the elastic modulus, whose changes are related to the onset and multiplication of microcracks), this is not so obvious with parameter q. A rearrangement of the two terms of Eq. 4 easily leads to (of course in a domain starting slightly above the yield point):

$$q = k\ \frac{d(\varepsilon)}{S_{AE}(\varepsilon)} \qquad\qquad \textbf{Eq. 5}$$

Thus q being constant should result in the ratio d/S_{AE} being also constant. Figure 5, in which the evolution of d has been plotted has a function of S_{AE}, evidences quasi straight lines for the three materials considered in the present study. Consequently, relating proportionally the microcracks density to the acoustic emission signal appears to be largely pertinent.

Therefore, when considering:

$$K'(\varepsilon) = q.K(\varepsilon).L_d(\varepsilon) \qquad\qquad \textbf{Eq. 6}$$

One finally obtains:

$$\frac{\Delta R(\varepsilon)}{R_0} = (1 + \alpha(\varepsilon).\varepsilon)[K'(\varepsilon).S_{AE}(\varepsilon) + 1] - 1 \qquad\qquad \textbf{Eq. 7}$$
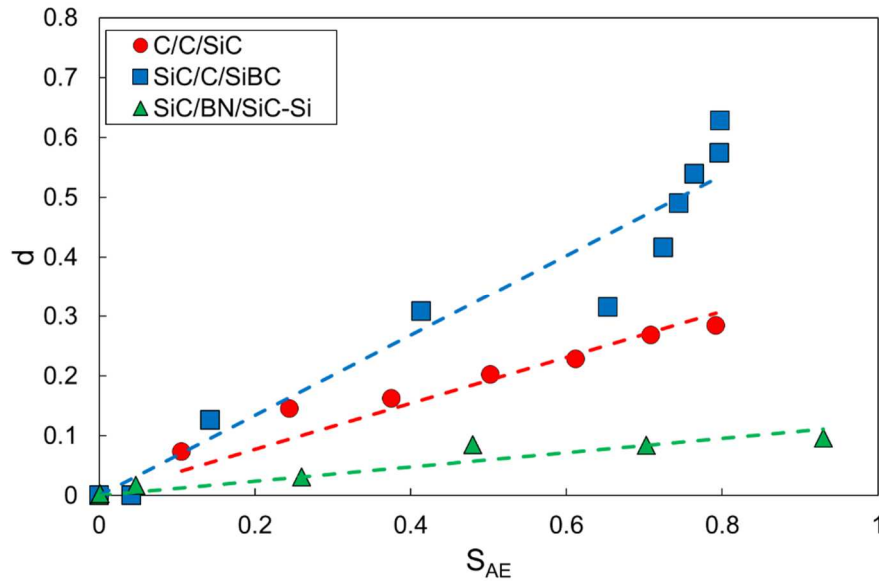
Figure 5. Evolution of the damage parameter _d_ as a function of the acoustic emission signal _S__{_AE_} for the three materials investigated.

4.2. *Application of the model*

In order to estimate the value of the piezo-resistivity of the composites, which may be chosen either constant or evolving with the strain, α(ε) is written as follows:

$$\alpha(\varepsilon) = f\big(\langle \varepsilon - \varepsilon_y \rangle\big) + \alpha_0 \qquad\qquad \textbf{Eq. 8}$$

With : α_0 the piezoresistance factor of the undamaged composite, ε_y the yield strain of the composite (*i.e.* the point at which damage starts to take place), <.> McAuley brackets defined by " $\forall x \in \mathbb{R}$, <x> = max(0,x)", f a function, positive and equal to zero at the origin.

From Eq. 7, it may be seen that, when no damage takes place (or does not evolve again), $S_{AE}(\varepsilon)$ is equal to zero as well as the term <ε-ε_y>, so that one obtains:

$$\frac{\Delta R(\varepsilon)}{R_0} = \alpha_0 \varepsilon \qquad\qquad \textbf{Eq. 9}$$

Thus, α_0 can be defined from the initial slope of the electric resistance/strain curves. Measured values are reported in the following table:

Composite material	C/C/SIC	SiC/C/SiBC	SiC/BN/SiC-Si
α_0	0.41 ± 0.1	2.30 ± 0.1	12.04 ± 0.2
ε_y (%)	0.04	0.1	0.1

Table 3. Initial piezoresistance factor of the three composites along with their tensile yield strain.

In order to determine function f, the beginning of the reloading part of the interposed unloading/reloading cycles (in terms of electrical resistance as a function of strain) were used. This means that, at each unloading sequence (down to zero stress), one has to consider a new material, damaged but with a microcracks density remaining constant up to a certain reloading threshold, which obeys to the scenario schematically displayed in Figure 4. The evolution of the piezoelectric coefficients as a function of strain, plotted according to Eq. 8, is exhibited in Figure 6.

It appears from the graphs plotted in this figure that the curves may be fairly fitted by either a quadratic or a linear function (linear in the case of the C/C/SiC and SiC/BN/SiC-Si composites, *i.e.* with variable a being equal to 0):

$$\alpha(\varepsilon) = a \langle \varepsilon - \varepsilon_y \rangle^2 + b \langle \varepsilon - \varepsilon_y \rangle + \alpha_0 \qquad\qquad \textbf{Eq. 10}$$
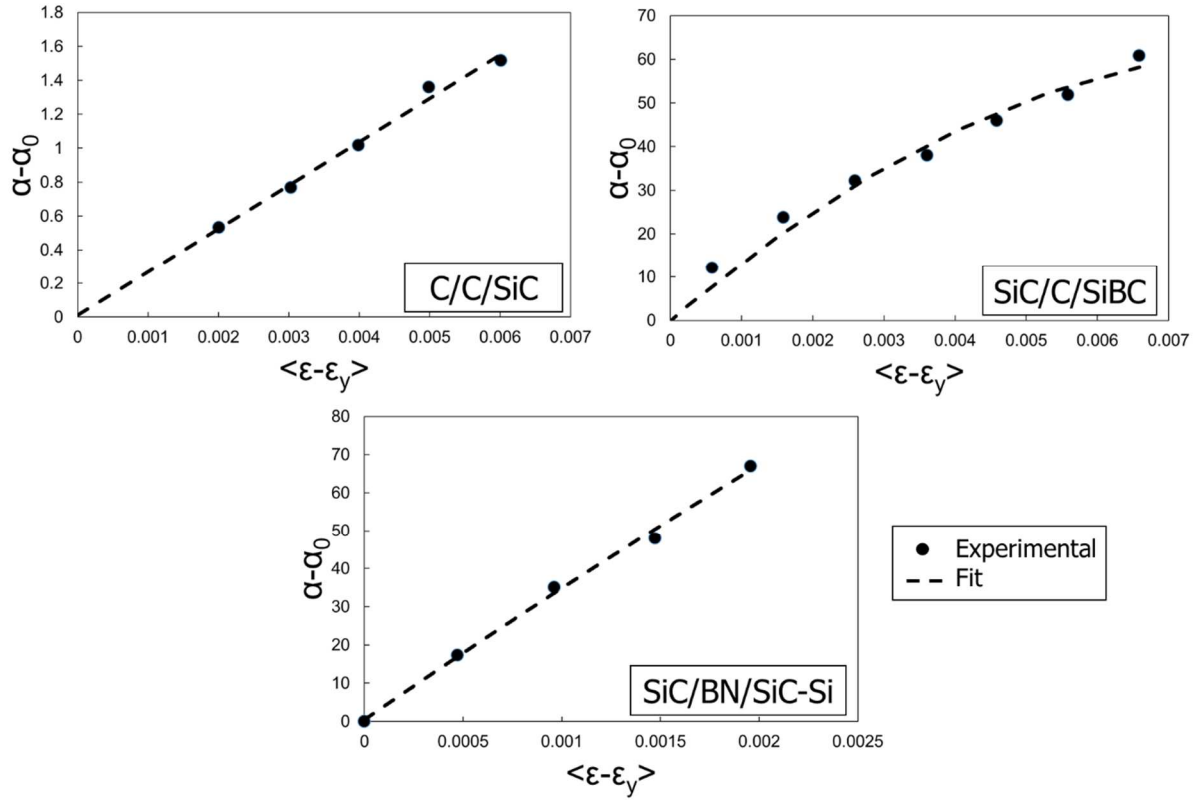
Figure 6. Evolution of the initial reloading elastic resistance obtained from the unloading/reloading cycles as a function of the strain (beyond the damage threshold).

Once the piezoelectric coefficient having been identified, it was then possible to use Eq. 7 in order to plot the evolution of K', expressed with the help of ΔR, α and S_{AE}, as a function of the strain. This has been done for the three materials with the two possibilities retained for α (*i.e.* either constant or evolving with the strain). Results have shown that, in both case, a quadratic function could also be used to fit the results (Figure 7). In other word, one always has:

$$\text{For } \varepsilon > \varepsilon_y, K'(\varepsilon) = a'\langle\varepsilon - \varepsilon_y\rangle^2 + b'\langle\varepsilon - \varepsilon_y\rangle + c' \qquad \textbf{Eq. 11}$$

As ascertained from Figure 8, both assumption made on the value of the piezoelectric factor α, *i.e.* either constant or evolving with the strain, leads to a similar possibility of fitting the relative evolution of the electric resistance. Therefore, one has to find another way of distinguishing between these two assumptions. This has been done by considering the average slope of the hysteretic loops induced by the unloading/reloading cycles derived from the electric resistance-strain curves.
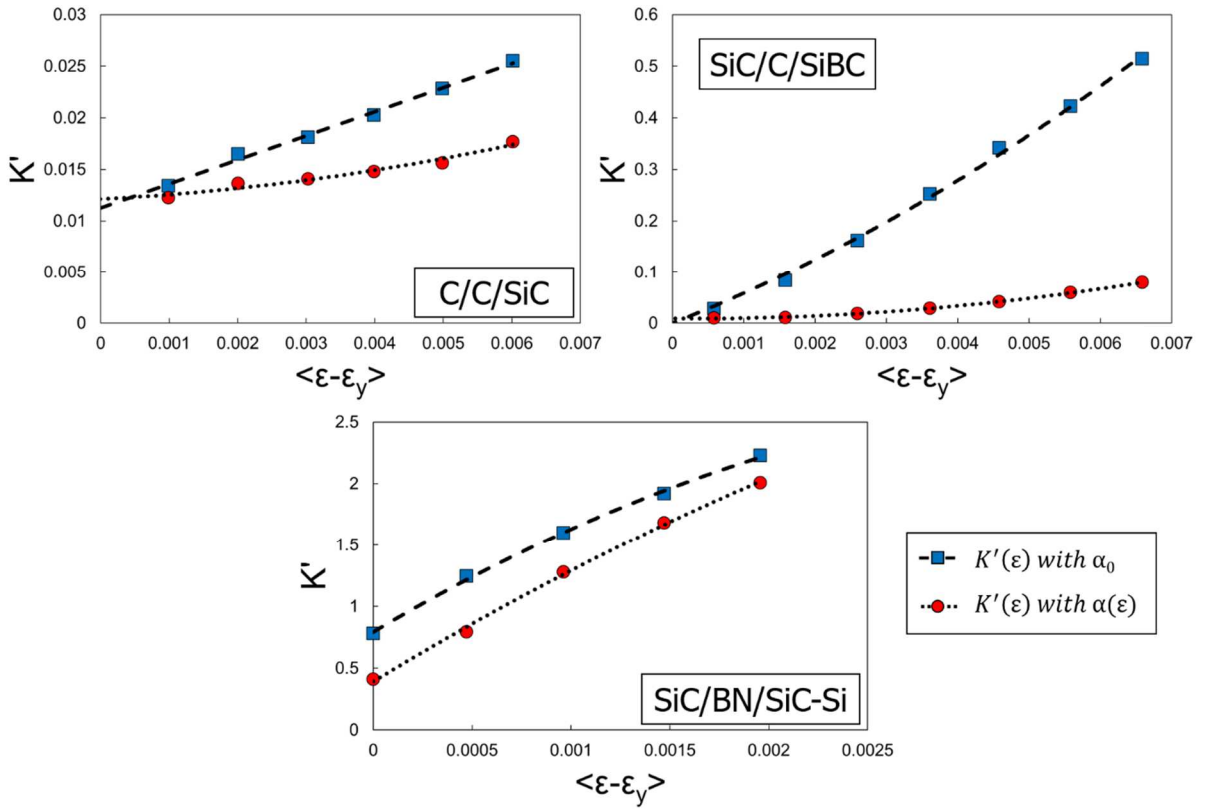
Figure 7. Evolution of K' as a function of the maximum strain reached at each cycle for either α constant or $\alpha(\varepsilon)$.
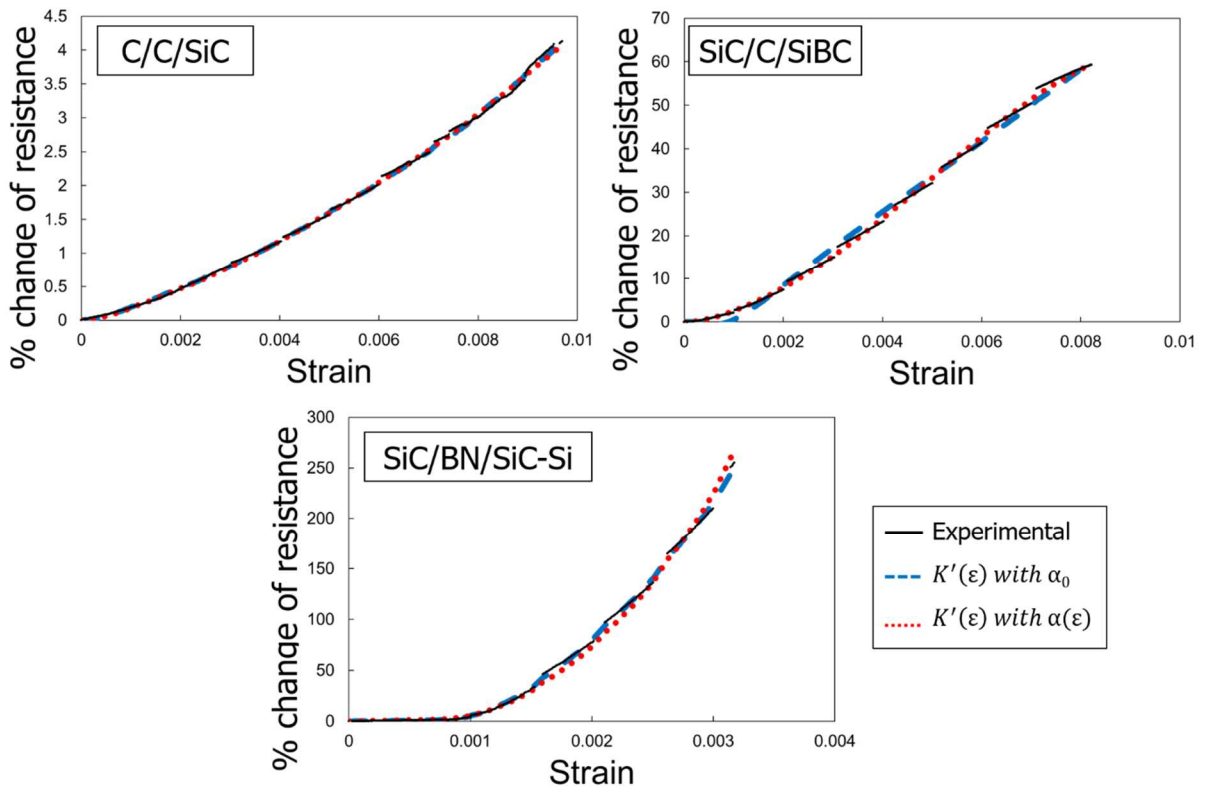

Figure 8. Relative variation of the electric resistance as a function of strain, for the three materials, along with their two possible representations.

16

Comparisons between predictions and experiments reported in Figure 9, show that, not surprisingly given the way that it has been assessed, the best fits are always obtained with an evolving piezoelectric factor α. The necessity of considering α et K' being sensitive to the strain, *i.e.* in fact to the damage present in the materials, is coherent with the basic hypothesis initially made regarding the use of elementary cell models whose parameters are sensitive to the various damaging processes. These results also confirm that the method used to identify $\alpha(\varepsilon)$ is suitable. The parameter K', which in fact allows to fit together the increases of both electric resistance and acoustic emission signal (see Eq. 6 and Eq. 7), logically evolves with the strain, for these two physical measurements are differently affected by damage, the former being more sensitive to crack opening [10,12]. The fact that K' always increases whatever the material considered highlights the progressive preponderance taken by crack opening (and related interfacial sliding) in the damage phenomena. This is in accordance with the observations made in the literature for the CMCs [2,15].
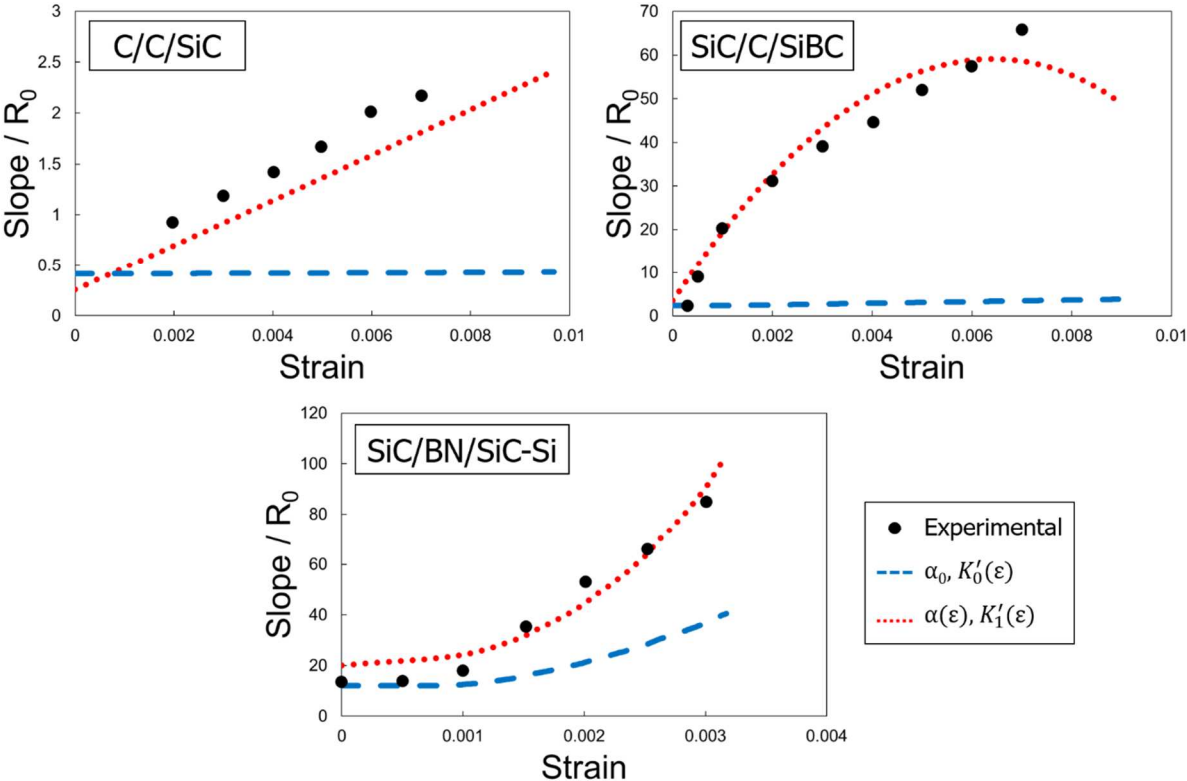

Figure 9. Average slope of the electric resistance-strain unloading/reloading hysteretic loops as a function of strain for the three materials, according to the model used.

5. Concluding remarks

The evolution of the electrical resistance of three ceramic matrix composites has been characterized in tension at room temperature. It has been shown that both the mechanical behavior and the evolution of the resistance as a function of the strain of these materials are strongly distinct.

A generic model linking the evolution of damage with that of the electrical resistance has then been proposed. It has been shown that this model is largely pertinent for the three different CMCs used in the present study, which provides strong hopes for its application to any kind of CMC. Although being mostly a fitting method aimed at conciliating acoustic emission signals and electrical resistance measures, this model is, yet quite simple, based on physically meaningful considerations. However, the present development of this model is only suitable for monotonic tension tests or for materials whose electrical resistance barely evolve upon interposed unloading/reloading cycles. It has thus been previously reported that this is not the case for SiC/C/SiBC composite, because of the modification of the electrical contacts that occur in the interphase during the cycles. Modelling the influence of interposed unloading/reloading cycles thus seems to be particularly interesting to investigate and may be the subject of further developments.

References

[1]   F. Christin, Design, Fabrication, and Application of Thermostructural Composites (TSC) like C/C, C/SiC, and SiC/SiC Composites, Adv. Eng. Mater. 4 (2002) 903–912. https://doi.org/10.1002/adem.200290001.

[2]   R. Naslain, Design, preparation and properties of non-oxide CMCs for application in engines and nuclear reactors: an overview, Compos. Sci. Technol. 64 (2004) 155–170. https://doi.org/10.1016/S0266-3538(03)00230-6.

[3]   E.P. Bouillon, P.C. Spriet, G. Habarou, C. Louchet, T. Arnold, G.C. Ojard, D.T. Feindel, C.P. Logan, K. Rogers, D.P. Stetson, Engine Test and Post Engine Test Characterization of Self-Sealing Ceramic Matrix Composites for Nozzle Applications in Gas Turbine Engines, in: American Society of Mechanical Engineers, 2004: pp. 409–416. https://doi.org/10.1115/GT2004-53976.

[4]   J.G. Sun, C.M. Deemer, W. Ellingson, J. Wheeler, NDT technologies for ceramic matrix composites: Oxide and nonoxide, Mater. Eval. 64 (2006) 52–60.

[5]   E. Maillet, C. Baker, G.N. Morscher, V.V. Pujar, J.R. Lemanski, Feasibility and limitations of damage identification in composite materials using acoustic emission, Compos. Part Appl. Sci. Manuf. 75 (2015) 77–83. https://doi.org/10.1016/j.compositesa.2015.05.003.

[6]   K. Schulte, Ch. Baron, Load and failure analyses of CFRP laminates by means of electrical resistivity measurements, Compos. Sci. Technol. 36 (1989) 63–76. https://doi.org/10.1016/0266-3538(89)90016-X.

[7]   J. Wen, Z. Xia, F. Choy, Damage detection of carbon fiber reinforced polymer composites via electrical resistance measurement, Compos. Part B Eng. 42 (2011) 77–86. https://doi.org/10.1016/j.compositesb.2010.08.005.

[8]   C.E. Smith, G.N. Morscher, Z.H. Xia, Monitoring damage accumulation in ceramic matrix composites using electrical resistivity, Scr. Mater. 59 (2008) 463–466. https://doi.org/10.1016/j.scriptamat.2008.04.033.

[9]   C.E. Smith, G.N. Morscher, Z. Xia, Electrical Resistance as a Nondestructive Evaluation Technique for SiC/SiC Ceramic Matrix Composites Under Creep-Rupture Loading: Resistance of SiC/SiC Under Creep-Rupture Loading, Int. J. Appl. Ceram. Technol. 8 (2011) 298–307. https://doi.org/10.1111/j.1744-7402.2010.02587.x.

[10] G.N. Morscher, C. Baker, C. Smith, Electrical Resistance of SiC Fiber Reinforced SiC/Si Matrix Composites at Room Temperature during Tensile Testing, Int. J. Appl. Ceram. Technol. 11 (2014) 263–272. https://doi.org/10.1111/ijac.12175.

[11] R. Mansour, E. Maillet, G.N. Morscher, Monitoring interlaminar crack growth in ceramic matrix composites using electrical resistance, Scr. Mater. 98 (2015) 9–12. https://doi.org/10.1016/j.scriptamat.2014.10.034.

[12] C. Simon, F. Rebillat, V. Herb, G. Camus, Monitoring damage evolution of SiCf/[SiBC]m composites using electrical resistivity: Crack density-based electromechanical modeling, Acta Mater. 124 (2017) 579–587. https://doi.org/10.1016/j.actamat.2016.11.036.

[13] Y.P. Singh, R. Mansour, G.N. Morscher, Combined acoustic emission and multiple lead potential drop measurements in detailed examination of crack initiation and growth during interlaminar testing of ceramic matrix composites, Compos. Part Appl. Sci. Manuf. 97 (2017) 93–99. https://doi.org/10.1016/j.compositesa.2017.03.006.

[14] C. Simon, F. Rebillat, G. Camus, Electrical resistivity monitoring of a SiC/[Si-B-C] composite under oxidizing environments, Acta Mater. 132 (2017) 586–597. https://doi.org/10.1016/j.actamat.2017.04.070.

[15] C.E. Smith, G.N. Morscher, Electrical resistance changes of melt infiltrated SiC/SiC loaded in tension at room temperature, Ceram. Int. 44 (2018) 183–192. https://doi.org/10.1016/j.ceramint.2017.09.157.

[16] T. Stäbler, H. Böhrk, H. Voggenreiter, Characterisation of electrical resistance for CMC materials up to 2000 K, Compos. Part Appl. Sci. Manuf. 112 (2018) 25–31. https://doi.org/10.1016/j.compositesa.2018.03.008.

[17] G.N. Morscher, R. Maxwell, Monitoring tensile fatigue crack growth and fiber failure around a notch in laminate SIC/SIC composites utilizing acoustic emission, electrical resistance, and digital image correlation, J. Eur. Ceram. Soc. 39 (2019) 229–239. https://doi.org/10.1016/j.jeurceramsoc.2018.08.049.

[18] H. Böhrk, P. Leschinski, T. Reimer, Electrical resistivity measurement of carbon-fiber-reinforced ceramic matrix composite under thermo-mechanical load, Compos. Sci. Technol. 76 (2013) 1–7. https://doi.org/10.1016/j.compscitech.2012.11.005.

[19] T. Sujidkul, C.E. Smith, Z. Ma, G.N. Morscher, Z. Xia, Correlating Electrical Resistance Change with Mechanical Damage in Woven SiC/SiC Composites: Experiment and Modeling, J. Am. Ceram. Soc. 97 (2014) 2936–2942. https://doi.org/10.1111/jace.13019.

[20] R.M. Sullivan, E.H. Baker, C.E. Smith, G.N. Morscher, Modeling the effect of damage on electrical resistivity of melt-infiltrated SiC/SiC composites, J. Eur. Ceram. Soc. 38 (2018) 4824–4832. https://doi.org/10.1016/j.jeurceramsoc.2018.07.015.

[21] H. Mei, L. Cheng, Damage analysis of 2D C/SiC composites subjected to thermal cycling in oxidizing environments by mechanical and electrical characterization, Mater. Lett. 59 (2005) 3246–3251. https://doi.org/10.1016/j.matlet.2005.05.052.

[22] C. Tang, Y. Bando, Y. Huang, S. Yue, C. Gu, F. Xu, D. Golberg, Fluorination and Electrical Conductivity of BN Nanotubes, J. Am. Chem. Soc. 127 (2005) 6552–6553. https://doi.org/10.1021/ja042388u.

[23] G. Camus, L. Guillaumat, S. Baste, Development of damage in a 2D woven C/SiC composite under mechanical loading: I. Mechanical characterization, Compos. Sci. Technol. 56 (1996) 1363–1372. https://doi.org/10.1016/S0266-3538(96)00094-2.

[24] J. Tracy, Multi-scale Investigation of Damage Mechanisms in SiC/SiC Ceramic Matrix Composites., phd thesis, University of Michigan, 2014.

[25] J.W. Hutchinson, H.M. Jensen, Models of fiber debonding and pullout in brittle composites with friction, Mech. Mater. 9 (1990) 139–163. https://doi.org/10.1016/0167-6636(90)90037-G.

[26] M.Y. He, B.-X. Wu, A.G. Evans, J.W. Hutchinson, Inelastic strains due to matrix cracking in unidirectional fiber-reinforced composites, Mech. Mater. 18 (1994) 213–229. https://doi.org/10.1016/0167-6636(94)90022-1.

[27] L. Guillaumat, Microfissuration des CMC : relation avec la microstructure et le comportement mécanique, phd thesis, Bordeaux 1, 1994. http://www.theses.fr/1994BOR10546 (accessed March 8, 2018).

[28] F. Hild, A. Burr, F.A. Leckie, Matrix cracking and debonding of ceramic-matrix composites, Int. J. Solids Struct. 33 (1996) 1209–1220. https://doi.org/10.1016/0020-7683(95)00067-4.

[29] H. Mei, Measurement and calculation of thermal residual stress in fiber reinforced ceramic matrix composites, Compos. Sci. Technol. 68 (2008) 3285–3292. https://doi.org/10.1016/j.compscitech.2008.08.015.